analytical chemistry

Article

Cite This: Anal. Chem. 2017, 89, 11552-11559

pubs.acs.org/ac

Monitoring of Heparin Activity in Live Rats Using Metal–Organic Framework Nanosheets as Peroxidase Mimics

Hanjun Cheng,[†] Yufeng Liu,[†] Yihui Hu,[†] Yubin Ding,[†] Shichao Lin,[†] Wen Cao,[†] Qian Wang,[†] Jiangjiexing Wu,[†] Faheem Muhammad,[†] Xiaozhi Zhao,[‡] Dan Zhao,[§] Zhe Li,[†] Hang Xing,*[,§] and Hui Wei*[,†]

[†]Department of Biomedical Engineering, College of Engineering and Applied Sciences, Collaborative Innovation Center of Chemistry for Life Sciences, Nanjing National Laboratory of Microstructures, Nanjing University, Nanjing, Jiangsu 210093, China

[‡]Department of Urology, Nanjing Drum Tower Hospital, The Affiliated Hospital of Nanjing University Medical School, Nanjing, Jiangsu 210008, China

[§]Institute of Chemical Biology and Nanomedicine, College of Chemistry and Chemical Engineering, Hunan University, Changsha, Hunan 410082, China

Supporting Information

ABSTRACT: Metal–organic framework (MOF) nanosheets are a class of two-dimensional (2D) porous and crystalline materials that hold promise for catalysis and biodetection. Although 2D MOF nanosheets have been utilized for *in vitro* assays, ways of engineering them into diagnostic tools for live animals are much less explored. In this work, a series of MOF nanosheets are successfully engineered into a highly sensitive and selective diagnostic platform for *in vivo* monitoring of heparin (Hep) activity. The iron-porphyrin derivative is selected as a ligand to synthesize a series of archetypical MOF nanosheets with intrinsic heme-like catalytic sites, mimicking peroxidase. Hep-specific AG73 peptides as recognition motifs are physically adsorbed onto MOF nanosheets, blocking active sites from nonspecific substrate–catalyst interaction. Because of the highly specific interaction between Hep and AG73, the activity of AG73-MOF nanosheets is restored upon the binding of Hep, but not Hep analogues and other endogenous biomolecules. Furthermore, by taking advantages of biocompatibility and diagnostic property enabled by AG73-MOF nanosheets, the elimination process of Hep in live rats is quantitatively monitored by coupling with microdialysis technology. This work expands the biomedical applications of 2D MOF nanomaterials and provides access to a promising *in vivo* diagnostic platform.

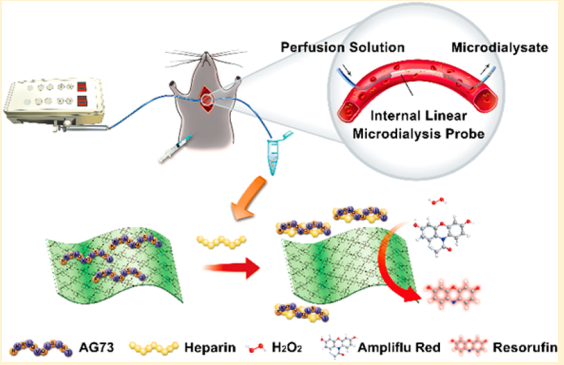

Nanomaterials with enzyme-like catalytic activities, known as "nanozymes", have received growing interest in the past decades.[1] Indeed, some intrinsic limitations arising from natural enzymes, such as low stability, high cost, and sensitivity to harsh environments, all can be overcome to some extent through the usage of nanozymes as a mimic. Up until now, nanozymes from different nanomaterials have successfully mimicked a series of natural enzymes, such as peroxidase, oxidase, catalase, superoxide dismutase, nuclease, and phosphatase,[1−15] which has enabled a variety of applications in research and medicine.[16−30] Particularly, some intriguing applications, such as rapid *E. bola* diagnosis and tumor immunostaining, have been achieved by peroxidase-mimicking nanomaterials.[3,24]

Among all materials that mimic enzyme activities, metal–organic frameworks (MOFs), a class of crystalline and porous materials formed by metal nodes and polydentate ligands, have emerged as promising biomimetic catalysts.[31−35] Some key features, such as multiple catalytic sites from either metal nodes and/or ligands with active sites, tailorable structures, high robustness to environment, and convenient recyclability, have extended the application region of MOFs over other materials.[31−35] Indeed, MOFs have been reported recently to mimic proteases for protein hydrolysis and to monitor glucose level in living brains as peroxidases mimics.[27,28,36−38] However, the potential drawback of bulk MOFs-based nanozymes is that only a small fraction of active sites is exposed on surface while the majority of them are hidden within the framework. Thus, the catalytic activities are significantly impaired due to the large diffusion barrier. In addition, the small surface-to-volume ratio of bulk MOF nanozymes limits the number of potential binding sites for interfacing biorecognition, which further limits their biodiagnostic applications. To improve the catalytic and biorecognition properties of MOF nanozymes, an effective strategy is to engineer bulk MOF structure into an ultrathin

Received: July 23, 2017
Accepted: October 10, 2017
Published: October 10, 2017

DOI: 10.1021/acs.analchem.7b02895
Anal. Chem. 2017, 89, 11552−11559

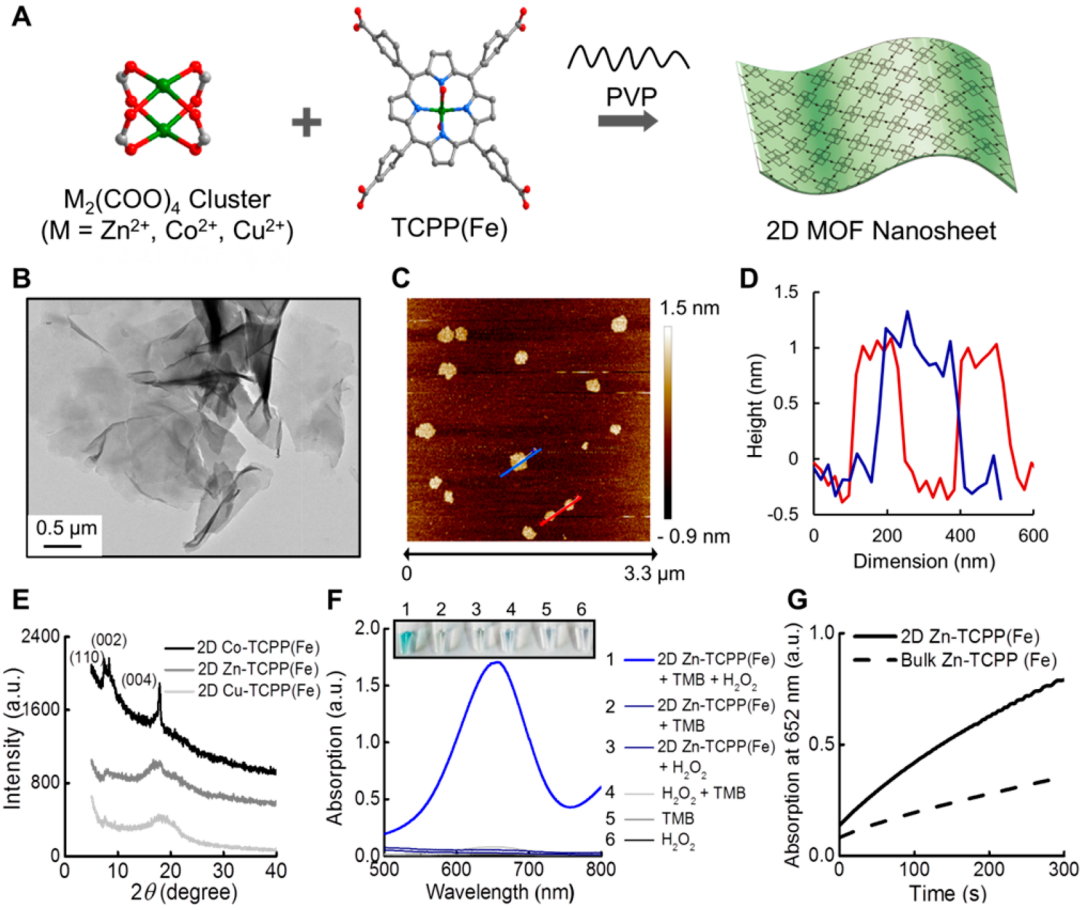

Figure 1. (A) Scheme showing the surfactant-assisted bottom-up synthesis of 2D MOF nanosheets. (B) TEM image of 2D Zn-TCPP(Fe) nanosheet. (C) AFM image of 2D Zn-TCPP(Fe) nanosheet and (D) the corresponding cross-sectional analysis of three pieces of nanosheets. The heights of all three pieces were estimated ~1−1.5 nm. (E) PXRD patterns of 2D Co-TCPP(Fe) (black), Zn-TCPP(Fe) (dark gray), and Cu-TCPP(Fe) (gray) nanosheets. (F) UV−visible absorption spectra of six sample solutions in 0.10 M acetate buffer (pH 5.0) containing (1) 2D Zn-TCPP(Fe) + TMB + H_2O_2, (2) 2D Zn-TCPP(Fe) + TMB, (3) 2D Zn-TCPP(Fe) + H_2O_2, (4) H_2O_2 + TMB, (5) TMB, (6) H_2O_2. Inset: corresponding photograph image of sample solutions in test tubes. (G) Kinetic curves plotting the time-dependent UV−vis absorbance at 652 nm of reactions catalyzed by 2D and 3D bulk Zn-TCPP(Fe) MOFs, showing the different catalytic properties.

two-dimensional (2D) MOF nanosheet.[31,32,34] The 2D MOF nanozymes surpass their bulk analogues for (i) highly exposed surface area with more accessible active sites for enzymatic catalysis and (ii) high density of binding sites for interacting with targets of interest. Though 2D MOF nanosheets have been reported as bioassays, ways of incorporating recognition motifs and further engineering those for *in vivo* biodiagnostic application are still challenging.

Herein, we describe the development of an *in vivo* bioassay using 2D MOF nanosheets as peroxidase mimics. A series of 2D MOFs were synthesized from binuclear paddle-wheel metal clusters and metalated tetrakis(4-carboxyphenyl)porphyrin (TCPP) ligands to mimic peroxidase. The prepared 2D MOF nanozymes possess enhanced peroxidase-mimicking activities than their 3D bulk analogues. Using TCPP metalated with different metal ions, we identified 2D MOF architecture consisting of Fe-bound TCPP (TCPP(Fe)) ligands exhibit the highest activity, demonstrating the dominant role of the heme-like ligands in determining the activities of nanozymes. As proof-of-concept of bioassay, antiheparin (Hep) peptides AG73 were physically adsorbed onto MOF nanosheets, modulating the enzymatic activity by interacting with peptides and Hep molecules. Furthermore, AG73-2D MOF as a sensitive and selective bioassay was demonstrated to monitor Hep elimination process in live rats.

EXPERIMENTAL SECTION

***In Vitro* Measurement of Hep.** To develop the 2D MOF-based bioassay for measurement of Hep, AG73 peptide (10 μg/mL) and 2D Zn-TCPP(Fe) nanosheets (5 μg/mL) were preincubated in 0.10 M acetate buffer (pH 5.0) for 5 min to form peptide/Zn-TCPP(Fe) nanocomposites. Then, different concentrations of Hep in Ringer's solution were added into the mixture and the resulting reaction solution was incubated at room temperature for another 40 min to allow complete binding between AG73 and Hep. Finally, the reacted solution was mixed with H_2O_2 and chromogenic substrate TMB or Ampliflu Red to allow UV−visible or fluorescent spectroscopic measurements. By using TMB as the reporting molecule, the obtained reaction mixtures containing 1 mM H_2O_2 and 500 μM TMB were allowed to UV−visible spectroscopic measurements by continuously monitoring the absorption changes at 652 nm. On the other hand, by using Ampliflu Red as the reporting molecule, the obtained reaction mixtures containing 1 mM H_2O_2 and 400 μM Ampliflu Red were allowed to fluorescent spectroscopic measurements by continuously monitoring the

DOI: 10.1021/acs.analchem.7b02895
Anal. Chem. 2017, 89, 11552−11559

fluorescence emission spectra at 585 nm with the excitation wavelength at 560 nm.

***In Vivo* Measurement of Hep in Live Rats.** The animal studies were approved by the Committee for Experimental Animals Welfare and Ethics of Nanjing Drum Tower Hospital, the Affiliated Hospital of Nanjing University Medical School. Adult male Sprague−Dawley rats (250−300 g) were purchased from Jiesijie Laboratory Animal Co. (Shanghai, China). Hep saline solution (0.9%) of 2 mL (100 μg/mL) was injected intraperitoneally. After dosing for 20 min, 1 mL of blood was first taken from the abdominal aorta of the rats and was then purified by perfusing the fluids through a microdialysis probe (CMA, 4 μm length) at 1.0 μL/min.

For the measurement of Hep in the blood of live rats, 10 μL of AG73 (100 μg/mL) and 0.8 μL of Zn-TCPP(Fe) (612 μg/mL) were added into 60 μL of 0.10 M acetate buffer (pH 5.0) and incubated for 5 min to prepare a fresh probe solution. Then, 20 μL of the sampled blood microdialysate was added into the probe solution and the resultant mixture was incubated for another 40 min. Finally, 10 μL of Ampliflu Red (4 mM) and 1 μL of H_2O_2 (100 mM) were added into the reaction mixture and the solution was immediately processed for fluorescent spectroscopic measurements by continuously monitoring the fluorescence emission at 585 nm with the excitation wavelength at 560 nm.

***In Vivo* Monitoring Hep Elimination Process.** The rats were first anesthetized with chloral hydrate (345 mg/kg, ip). Then, through a midline cervical incision, both common carotid arteries were exposed and isolated from surrounding connective tissue. A linear microdialysis probe (CMA) was then carefully embedded in one carotid artery. Note, particular care was needed to avoid damaging the vagus and the sympathetic nerves close by. The linear microdialysis probe was perfused with Ringer's solution at 1 μL/min. The perfusion was run for at least 60 min to achieve equilibration before collection of microdialysis sample. After equilibration, the rat was administrated with Hep by intraperitoneal injection of 2 mL of Hep saline solution (100 μg/mL). Throughout the surgery, the body temperature of the animals was maintained at 37 °C using a heating pad.

Instrumentation. Powder X-ray diffraction (PXRD) data were collected on an ARL SCINTAG X'TRA diffractometer using Cu Kα radiation (Thermo). Transmission electron microscopy (TEM) was performed on a Tecnai F20 transmission electron microscope (FEI) at an acceleration voltage of 200 kV. The hydrodynamic size of 2D Zn-TCPP(Fe) nanosheet was measured on a Nanosizer ZS90 (Malvern). UV−visible absorption spectra were collected on a UV−visible spectrophotometer with a 1 cm quartz cell (Beijing Purkinje General Instrument Co. Ltd., China). Fluorescent spectra were obtained on a Hitachi F-4600 fluorescent spectrometer (Japan).

RESULTS AND DISCUSSION

Synthesis of 2D MOF Nanosheets and Evaluation of Their Peroxidase-like Activities. To design a 2D MOF nanosheet mimicking peroxidase, both the MOF structure as a whole and the active sites within the network need to be considered. A type of 2D MOF structures consisting of binuclear paddle-wheel inorganic units (e.g., Zn^{2+}, Co^{2+}, and Cu^{2+}) and heme-like metalloporphyrin polydentate organic ligands (e.g., TCPP(Fe)) was selected as model system (Figure 1A).[31,32] In this type of structure, both organic and inorganic building blocks feature planar 4-connectivity, ensuring the growth of the coordination network into a 2D plane rather than a 3D extended structure. In addition, as heme is a cofactor for natural peroxidases, it is expected that the incorporated metalloporphyrins would be able to render the MOF structure with required peroxidase mimicking activities.[39] The 2D MOF nanozymes consisting of divalent metal ions Zn^{2+}, Co^{2+}, or Cu^{2+} and ligand TCPP(Fe) (termed as 2D Zn-TCPP(Fe), 2D Co-TCPP(Fe), and 2D Cu-TCPP(Fe)) were prepared via a surfactant-assisted strategy, where PVP was used as surfactant to confine the growth of MOF crystal into two dimensions. Transmission electron microscopy (TEM) was used to visualize the structure of prepared MOFs. As shown in Figure 1B and Figure S1, all three 2D MOFs exhibited well-defined ultrathin sheet-like structures. The 2D sheet structure of 2D Zn-TCPP(Fe) was further studied by atomic force microscopy (AFM) (Figure 1C). The thickness of 2D Zn-TCPP(Fe) was estimated ∼1−1.5 nm (Figure 1D), indicating only a few molecular layers were stacked. The crystalline feature of these 2D MOF nanozymes was characterized by powder X-ray diffraction (PXRD). As shown in Figure 1E, all MOFs displayed three feature peaks at 7.6°, 8.8°, and 17°, which were indexed as (110), (002), and (004), respectively, suggesting the assembled (4, 4) 2D network.[31,32]

The peroxidase-mimicking activities of the prepared 2D MOF nanozymes were evaluated through the oxidation of peroxidase chromogenic substrate 3,3′,5,5′-tetramethylbenzidine (TMB) with H_2O_2 and characterized by UV−visible spectroscopy (UV−vis). As shown in Figure 1F, the introduction of the 2D Zn-TCPP(Fe) into 0.10 M acetate buffer (pH 5.0) containing both H_2O_2 and TMB resulted in an immediate color change from colorless to blue with a characteristic UV−vis absorption peak of oxidized TMB (TMB_{ox}) centered at 652 nm. In contrast, the combination of any of the two components did not generate color change, demonstrating the peroxidase-mimicking activity of the 2D MOF nanozyme. The kinetics of enzymatic reaction among three 2D MOF nanosheets (Zn-TCPP(Fe), Co-TCPP(Fe), and Cu-TCPP(Fe)) were further studied by monitoring the characteristic absorption peak of TMB_{ox} centered at 652 nm. All three nanozymes with different metal nodes exhibited comparable kinetic curves in 300 s with no significant differences of the catalytic activities observed, indicating metal nodes may have no correlation with the enzymatic property (Figure S2).

To systematically identify whether the catalytic activities of 2D MOF nanozymes are stemmed from their chelated metal ions or from their heme-like metalloporphyrin ligands, experiments studying the effects of metal nodes in MOF structure and porphyrin-coordinated metal ions were carried out. To study the effect of metal nodes and minimize the influence of the porphyrin center, three 2D MOF nanosheets (Zn-TCCP, Co-TCCP, and Cu-TCCP) were synthesized using TCPP ligand with empty porphyrin core. Ultrathin 2D sheet structures were observed for all three MOFs under TEM images (Figure S3). Peroxidase-mimicking activities of all three MOFs were monitored using the same method described above. As shown in Figure S4, all three MOFs with empty porphyrin core exhibited extremely low catalytic activities, invalidating the possibility of an active metal nodes in MOF (Figure S4). To study the effect of porphyrin-coordinated metal ions, TCPP(Zn), TCPP(Co), and TCPP(Mn) in addition to TCPP(Fe) were used to prepare 2D MOF structures with Zn^{2+} cluster as the metal nodes. Interestingly, Zn-TCPP(Zn) and

DOI: 10.1021/acs.analchem.7b02895
Anal. Chem. 2017, 89, 11552−11559

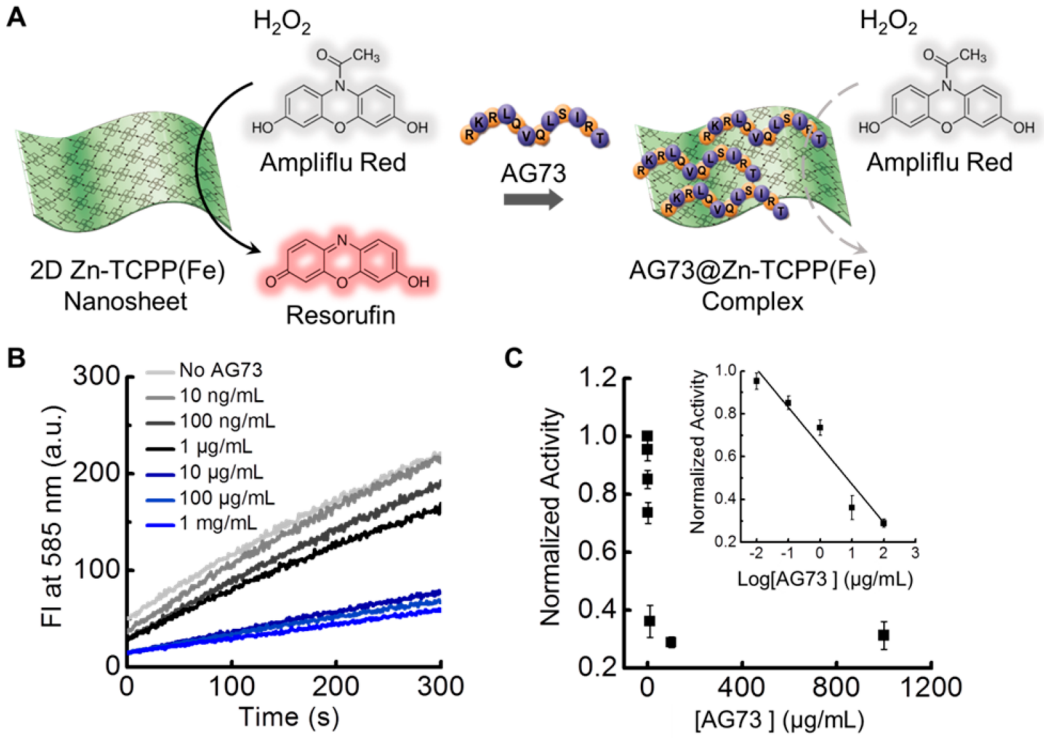

Figure 2. (A) Schematic illustration of AG73-inhibited peroxidase-like activity of 2D Zn-TCPP(Fe) nanosheets with Ampliflu Red as the redox substrate. (B) Kinetic curves plotting the time-dependent fluorescence emission intensity at 585 nm (FI_{585}) for Ampliflu Red oxidation reactions catalyzed by Zn-TCPP(Fe) in different AG73 concentrations. The reactions were processed in 0.10 M acetate buffer (pH 5.0) containing 400 μM Ampliflu Red, 1 mM H_2O_2, and 5 μg/mL 2D Zn-TCPP(Fe) nanosheets. (C) Normalized catalytic activity of 2D Zn-TCPP(Fe) nanosheets in different AG73 concentrations. The catalytic activity decreases with the increase of peptide concentration. Inset: plot of normalized activity versus the logarithm of the AG73 concentration, showing a linear relationship in low concentration range.

Zn-TCPP(Co) exhibited similar sheet-like 2D structures to Zn-TCPP(Fe), while the obtained Zn-TCPP(Mn) tended to form nanobelt morphology (Figure S5). The enzymatic activity studies clearly showed that none of the MOF structures have comparable peroxidase-mimicking activities to Zn-TCPP(Fe), the activity of which is ~7−20 times higher than MOFs with non-Fe porphyrin ligands (Figure S6). This is expected because the Fe center serves as the active site in natural peroxidase. Taken together, these results support the conclusion that the TCPP ligand played a dominant role in determining the peroxidase-mimicking activities of 2D MOF nanozymes while the connecting metal nodes mainly serve as structural building blocks, i.e., the porphyrin center-like TCPP ligands acted as the active sites in 2D MOF nanosheets. For all the MOF structures studied, the ones containing TCPP(Fe) exhibited the highest catalytic activities. As 2D Zn-TCPP(Fe) was among the best peroxidase mimics discussed above, it was used as a model material for further studies.

To study the advantages of 2D MOF nanosheet, a 3D bulk analogue was prepared from Zn^{2+} and TCPP(Fe) in the absence of PVP. As shown in Figure S7A, the 3D Zn-TCPP(Fe) exhibited microsized irregular morphology. The PXRD diffraction patterns of 2D and 3D Zn-TCPP(Fe) matched well with each other, indicating the same crystalline structure (Figure S7B). The peroxidase-mimicking activity of 3D Zn-TCPP(Fe) was investigated and compared with that of 2D Zn-TCPP(Fe). As shown in Figure 1G and Figure S8, a faster kinetic rate and a 2 times higher catalytic activity of 2D Zn-TCPP(Fe) than these of 3D Zn-TCPP(Fe) were observed. The results indicate that by engineering 3D MOFs into 2D ones, their peroxidase-mimicking activities can be significantly enhanced. Such enhancement is possibly attributed to larger exposed surface area with more accessible catalytic sites (i.e., the TCPP(Fe)) and less diffusion barrier of 2D Zn-TCPP(Fe) nanosheets.[31,32]

Tuning Peroxidase-Like Activity of 2D Zn-TCCP(Fe) Using Anti-Hep AG73 Peptide. After systematically studying the structural-activity relationship of 2D MOF nanozymes, Zn-TCPP(Fe) with the highest peroxidase-mimicking activity was chosen as a model complex for bioassay development. To develop an enzymatic bioassay, the activity of enzyme should be designed under quenching mode in the absence of targets and restored in the presence of targets. As proof-of-concept of bioassay development, a negatively charged linear glycosaminoglycan, Hep, was chosen as the target of interest. As an anticoagulant medication, Hep prevents deep vein thrombosis at right dosage but induces severe side effects if overdose occurs.[40−42] Also, thus there is a need for real-time monitoring the elimination process of Hep.[43−46]

To achieve target-specific activation of the enzymatic property on MOF, a Hep-specific binding peptide AG73 with the sequence of RKRLQVQLSIRT and isoelectric point (pI) of 12.4 was immobilized onto 2D Zn-TCPP(Fe) surface through physical adsorption.[44,47] To confirm the immobilization of peptides on the 2D MOF surface, we probed the surface charge of 2D Zn-TCPP(Fe) nanosheets with the addition of AG73. As shown in Figure S15, the ζ-potential of unmodified 2D Zn-TCPP(Fe) nanosheets was −15.3 mV, mainly attributed to the uncoordinated carboxyl groups on surface. The addition of AG73 led to an increment of the resultant ζ-potential. Since the

DOI: 10.1021/acs.analchem.7b02895
Anal. Chem. 2017, 89, 11552−11559

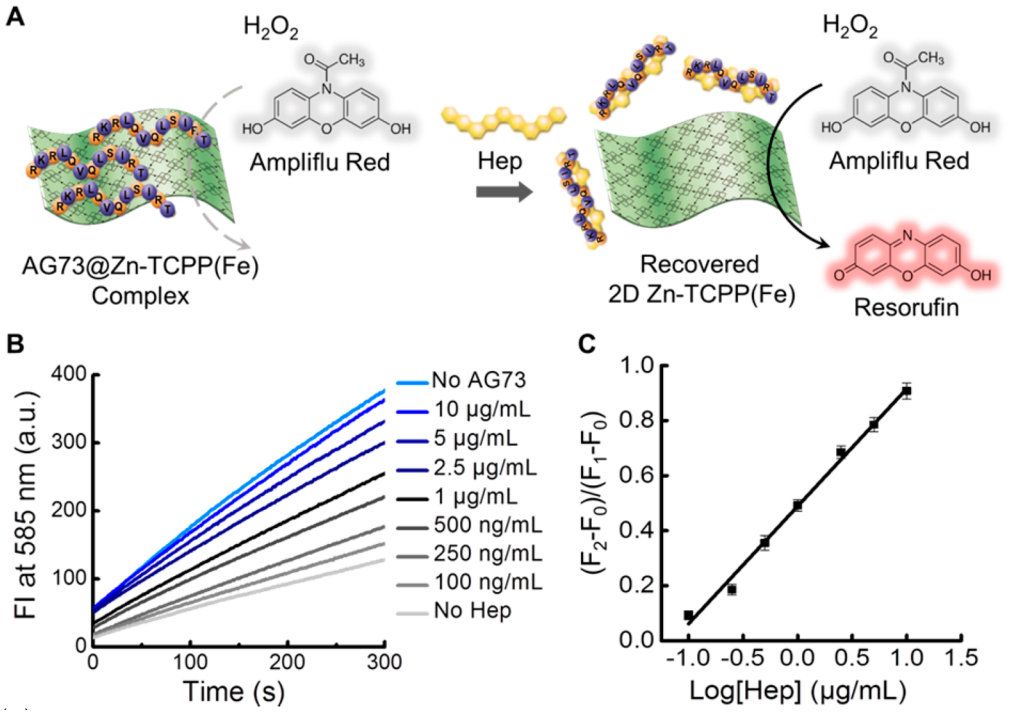

Figure 3. (A) Schematic illustration of AG73-modifed 2D MOF-based bioassay for Hep detection. (B) Kinetic curves plotting the time-dependent fluorescence emission intensity at 585 nm for Ampliflu Red oxidation reactions catalyzed by AG73-2D Zn-TCPP(Fe) in response to different Hep concentrations. The reactions were carried out in 0.10 M acetate buffer (pH 5.0) containing 400 μM Ampliflu Red, 1 mM H_2O_2, 5 μg/mL 2D Zn-TCPP(Fe) nanosheets, 10 μg/mL AG73, and different concentrations of Hep. (C) Plot of fluorescence intensity change ratio $(F_2 - F_0)/(F_1 - F_0)$ versus the logarithm of the Hep concentration. F_0, the FI_{585} in the presence of AG73; F_1, the FI_{585} values in the absence of Hep and AG73; F_2, the FI_{585} values in the presence of Hep and AG73. Error bars indicate standard deviations of three independent measurements.

net charge of the peptide is estimated to be positive under the experimental conditions, we attribute the ζ-potential change of MOF nanosheets to the electrostatic binding of AG73 to 2D Zn-TCPP(Fe) nanosheets. In addition, the ζ-potential of the AG73-2D Zn-TCPP(Fe) complex was ~+15.1 mV after adding 10 μg/mL AG73 and reached a plateau with higher peptide concentration, suggesting that the adsorption of AG73 onto 2D Zn-TCPP(Fe) nanosheets was saturated.

To study the impact of AG73 modification on the peroxidase-like activity of 2D Zn-TCPP(Fe) nanosheets, the kinetics and activity profile of the enzymatic reaction were studied by varying the AG73 concentration and keeping the MOF concentration constant (Figure 2A). Ampliflu Red or TMB as a peroxidase substrate was used as signal readout (Figure 2A and Figure S16). As shown in Figure 2B,C, higher AG73 concentration resulted in a slower catalytic rate and a lower peroxidase-like activity, indicating the adsorption of AG73 on the nanosheet surface shields the catalytic sites. The AG73-induced inhibition of peroxidase-like activity of MOF reached a plateau after the addition of 10 μg/mL AG73, which matches well with ζ-potential measurements, confirming AG73 adsorption reached the equilibrium state (Figure 2C).

To further understand the peptide−MOF interaction, activities of free TCPP(Fe) ligands and bulk Zn-TCPP(Fe) MOFs modulated by AG73 of different concentrations were studied (Figure S17). For free TCPP(Fe), the catalytic activity remained almost unchanged in the presence of AG73 in the tested concentration range, suggesting the negligible peptide−ligand interaction. For bulk Zn-TCPP(Fe) MOF, the peroxidase-mimicking activity increased with the increase of AG73 concentrations, which can be attributed to peptide-promoted solubilization of MOF particles. Taken together, the data suggest the activity of 2D Zn-TCPP(Fe) nanosheets can be modulated by a Hep-specific peptide but not the free Fe-porphyrin ligand or the bulk MOF particle, supporting our hypothesis of using 2D Zn-TCPP(Fe) for bioassay development.

Detection of Hep with 2D Zn-TCPP(Fe) Nanozyme. Having demonstrated the anti-Hep peptide AG73-modified 2D Zn-TCPP(Fe) nanosheets with quenched peroxidase-like activity, we then explored their Hep-specific activation and application as competitive bioassay for Hep detection. Figure 3A shows the Hep detection process using Ampliflu Red as the redox substrate for reporting signal. In the absence of Hep, the activity of peptide-modified MOF was quenched with minimum fluorescence emission. After the addition of Hep, AG73 peptides on MOF surface were able to specifically recognize Hep, destabilize the peptide−MOF interaction, and trigger the AG73 release from the surface of AG73-2D Zn−TCPP(Fe) complex, resulting in the recovery of peroxidase-like activity and increased fluorescence signal. The recovered peroxidase-like activity was measured by monitoring the time-dependent fluorescence intensity of Resorufin (i.e., the oxidized product of Ampliflu Red) at 585 nm, which is positively correlated to the target Hep concentration (Figure 3B). As shown in Figure 3C, a more quantitative analysis was carried out by plotting the ratios of fluorescence intensity change ($(F_2 - F_0)/(F_1 - F_0)$) after adding Hep versus the logarithm of Hep concentrations. A fit of the data indicates a linear response curve ranging from 0.1−10 μg/mL Hep with the slope of ~0.43 and a y-intercept of ~0.49 (R^2 = 0.991). The detection limit was further determined to be ~15 ng/mL ($S = 3\sigma$). These data

DOI: 10.1021/acs.analchem.7b02895
Anal. Chem. 2017, 89, 11552−11559

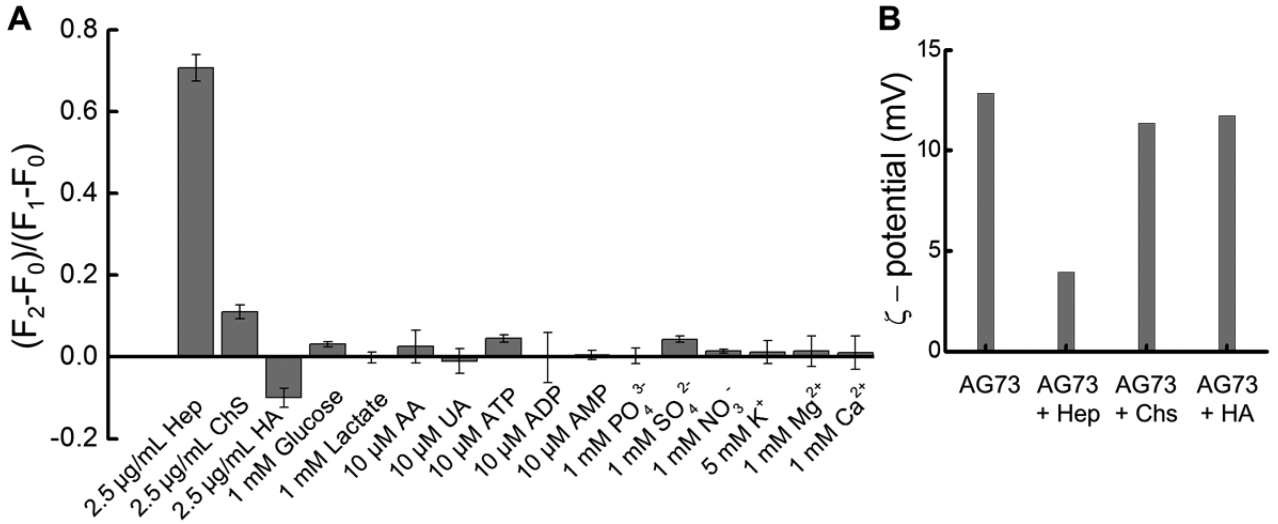

Figure 4. (A) Selectivity of the AG73-2D Zn-TCPP(Fe) bioassay toward Hep detection. Bars represent the fluorescence change ratio after adding of Hep and other interfering molecules. Error bars indicate standard deviations of three independent measurements. (B) ζ-potentials of AG73-2D Zn-TCPP(Fe) nanocomplex measured in the absence or the presence of Hep, ChS, or HA, respectively.

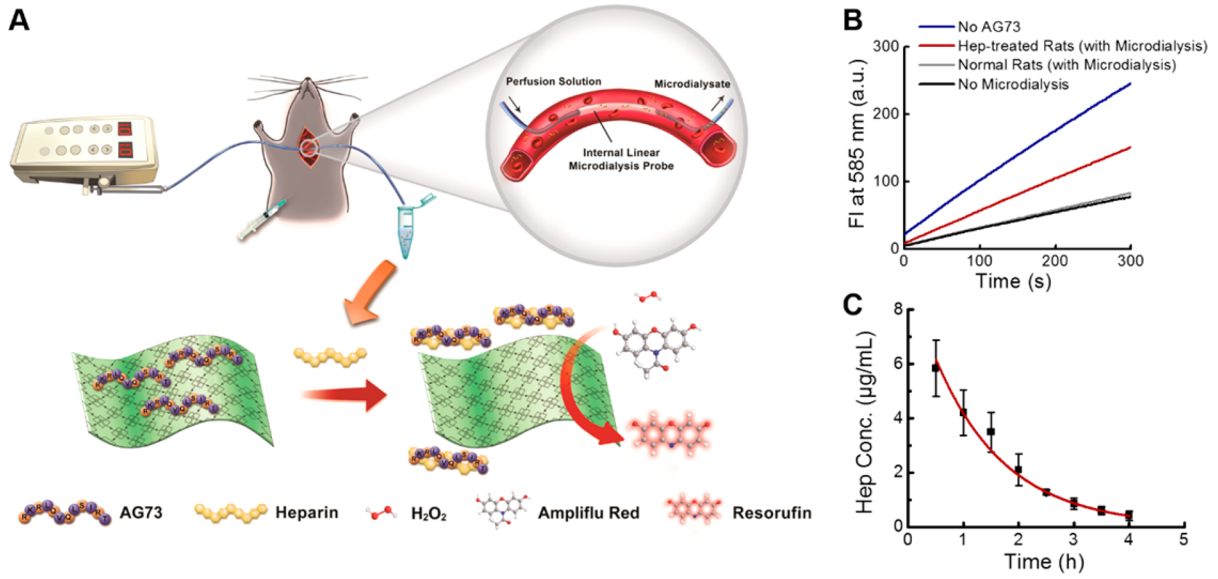

Figure 5. (A) Scheme showing the monitoring of Hep elimination process in live rats using 2D MOF nanozymes. (B) Kinetic curves plotting the time-dependent fluorescence intensity at 585 nm for three different samples mixing with AG73-modified MOFs and redox substrate: (red curve) microdialyzed serum from Hep-treated rats, (gray curve) microdialyzed serum from normal rats, and (black curve) negative control sample with no serum. (C) Dynamic changes of Hep concentrations in the artery of live rats over 4 h following the administration of Hep. A fitting of the data indicates an exponential decay. Error bars indicate standard deviations of three independent measurements.

suggest that the developed bioassay satisfies the requirements of monitoring Hep in clinical samples with concentrations ranging from 1.1 to 6.5 μg/mL during postoperative and long-term care.[48,49]

To allow monitoring Hep concentration in physiological conditions, such as in live animals, the developed bioassay must have high selectivity toward the target. To evaluate the selectivity of the 2D MOF-based bioassay, a variety of common biological interfering species were tested for their effects on nanozyme activation, including Hep analogues (chondrotin sulfate (CS) and hyaluronic acid (HA)), bioactive small molecules (glucose, lactate, ascorbic acid (AA), uric acid (UA), adenosine triphosphate (ATP), adenosine diphosphate (ADP), adenosine monophosphate (AMP)), and biologically important anions and cations (PO_4^{3-}, SO_4^{2-}, NO_3^-, K^+, Mg^{2+}, and Ca^{2+}). As shown in Figure 4A, none of them showed high fluorescence change ratio, indicating minimum interference for Hep detection. The selectivity of developed bioassay for Hep was also confirmed by ζ-potential measurements. Only Hep decreased the ζ-potential of the AG73-2D Zn-TCPP(Fe) nanocomplex but not analogues, confirming the highly specific recognition capacity of AG73 toward Hep. However, high concentration of BSA (5 mg/mL) as representative of serum protein was also observed to increase enzymatic activity, possibly due to the BSA-promoted solubilization of 2D Zn-TCPP(Fe) (Figure S18).

To eliminate the potential interference from serum proteins when applying the developed bioassay for Hep detection in live rats, microdialysis technology was used to treat serum sample before the measurement. We first tested the rat serum samples

DOI: 10.1021/acs.analchem.7b02895
Anal. Chem. 2017, 89, 11552−11559

spiked with different concentrations of Hep (i.e., 5, 10, and 20 μg/mL) after microdialysis to validate the performance of microdialysis. As shown in Figure S19 and Table S1, after microdialysis, the 2D MOF bioassay responded normally to all three Hep-spiked serum samples with a consistent ~65% detection recovery of spiked concentration. Next, to further demonstrate the feasibility of using developed bioassay for detecting Hep in live animals, Hep (100 μg/mL, 2 mL) in 0.9% normal saline was dosed intraperitoneally to rats and the blood samples were collected 20 min after dosage. The collected blood samples were microdialyzed and then diluted 4-fold with 0.10 M acetate buffer (pH 5.0) for measurements. The average Hep concentration in live rats was determined to be 4.47 ± 0.73 μg/mL (Table S2), which is consistent with previous reports studying Hep metabolism,[43] validating the use of 2D MOF bioassay for in vivo diagnostic applications.

The Hep elimination process in live rats was monitored by using the AG73-modified MOF bioassay in combination with the microdialysis probe. Figure 5A shows the design of the animal experiment. A linear microdialysis probe was carefully embedded in the artery of live rats and the corresponding microdialysates were continuously collected after the rats were intraperitoneally administered with Hep (Figure 5A). A kinetic study of the nanozyme catalytic reaction showed that microdialyzed serum from Hep-treated rats significantly activated AG73-modified MOF nanozymes while microdialyzed serum from normal rats or negative control sample with no serum did not (Figure 5B), suggesting a selective response of the bioassay. The elimination process of the Hep was investigated by plotting the time course of Hep concentrations in the artery of live rats over 4 h following administration (Figure 5C). As shown in Figure 5C, after the rats were intraperitoneally injected with Hep for 0.5 h, the Hep concentration in the artery was determined to be 5.84 ± 1.04 μg/mL and gradually decreased overtime to 0.41 ± 0.17 μg/mL after 4 h due to the elimination of Hep, which is possibly through depolymerization into smaller fragments by the reticuloendothelial system or urine from the renal route.[50,51] A fitting of the time course data indicates an exponential decay of Hep in serum of Hep in serum from 0.5−4 h after administration, which matches well with previous pharmacokinetic studies,[46,51,52] suggesting the successful application of the developed bioassay to monitor Hep in live rats.

CONCLUSIONS

In summary, we developed a highly sensitive and selective peptide-modified 2D MOF nanosheet as a diagnostic probe for Hep. Hep-specific peptide AG73 modification provided MOF nanosheets with target-responsive catalytic activity, through the stronger peptide−Hep interactions than peptide−MOF interactions. MOFs with different metal nodes, porphyrin-coordinated metal ions, and particle dimensions are studied to optimize the nanozymes properties and to understand the catalysis mechanism. Most notably, we have shown that the developed 2D MOF-based bioassay successfully monitored the dynamic changes of Hep in the artery of live rats after drug administration. The 2D MOF nanosheets bioassay described herein provides a general platform that can potentially be used for direct detection of many other biotargets in addition to Hep.

ASSOCIATED CONTENT

Supporting Information

The Supporting Information is available free of charge on the ACS Publications website at DOI: 10.1021/acs.analchem.7b02895.

Additional experimental details; supplementary figures about TEM images, selected-area electron diffraction patterns, zeta-potentials, and kinetic analysis; supplementary tables about recovery results of microdialysis, Hep determination in rats' blood, and kinetic parameters; and references (PDF)

AUTHOR INFORMATION

Corresponding Authors

*E-mail: weihui@nju.edu.cn. Phone: +86-25-83593272. Fax: +86-25-83594648.

*E-mail: hangxing@hnu.edu.cn.

ORCID

Hui Wei: 0000-0003-0870-7142

Author Contributions

The manuscript was written through contributions of all authors. All authors have given approval to the final version of the manuscript.

Notes

The authors declare no competing financial interest.

ACKNOWLEDGMENTS

This work was supported by National Natural Science Foundation of China (Grants 21722503, 21405081, and 21405079), Natural Science Foundation of Jiangsu Province (Grant BK20160615), 973 Program (Grant 2015CB659400), Shuangchuang Program of Jiangsu Province, Open Funds of the State Key Laboratory of Analytical Chemistry for Life Science (Grant SKLACLS1704), Open Funds of the State Key Laboratory of Coordination Chemistry (Grant SKLCC1619), China Postdoctoral Science Foundation (Grant 2016M590437), and Thousand Talents Program for Young Researchers. The authors thank Dr. Meiting Zhao for her assistance on 2D MOF synthesis.

REFERENCES

(1) Wei, H.; Wang, E. *Chem. Soc. Rev.* **2013**, *42*, 6060−6093.

(2) Gao, L. Z.; Zhuang, J.; Nie, L.; Zhang, J. B.; Zhang, Y.; Gu, N.; Wang, T. H.; Feng, J.; Yang, D. L.; Perrett, S.; Yan, X. *Nat. Nanotechnol.* **2007**, *2*, 577−583.

(3) Fan, K. L.; Cao, C. Q.; Pan, Y. X.; Lu, D.; Yang, D. L.; Feng, J.; Song, L. N.; Liang, M. M.; Yan, X. Y. *Nat. Nanotechnol.* **2012**, *7*, 459−464.

(4) Zhang, Z.; Zhang, X.; Liu, B.; Liu, J. *J. Am. Chem. Soc.* **2017**, *139*, 5412−5419.

(5) Liu, B. W.; Sun, Z. Y.; Huang, P. J. J.; Liu, J. W. *J. Am. Chem. Soc.* **2015**, *137*, 1290−1295.

(6) Manea, F.; Houillon, F. B.; Pasquato, L.; Scrimin, P. *Angew. Chem., Int. Ed.* **2004**, *43*, 6165−6169.

(7) Chen, J. L. Y.; Pezzato, C.; Scrimin, P.; Prins, L. J. *Chem. - Eur. J.* **2016**, *22*, 7028−7032.

(8) Zhang, W.; Hu, S. L.; Yin, J. J.; He, W. W.; Lu, W.; Ma, M.; Gu, N.; Zhang, Y. *J. Am. Chem. Soc.* **2016**, *138*, 5860−5865.

(9) Shen, X.; Liu, W.; Gao, X.; Lu, Z.; Wu, X.; Gao, X. *J. Am. Chem. Soc.* **2015**, *137*, 15882−15891.

(10) Natalio, F.; Andre, R.; Hartog, A. F.; Stoll, B.; Jochum, K. P.; Wever, R.; Tremel, W. *Nat. Nanotechnol.* **2012**, *7*, 530−535.

DOI: 10.1021/acs.analchem.7b02895
Anal. Chem. 2017, 89, 11552−11559

(11) Karakoti, A.; Singh, S.; Dowding, J. M.; Seal, S.; Self, W. T. *Chem. Soc. Rev.* **2010**, *39*, 4422−4432.
(12) Lin, Y.; Ren, J.; Qu, X. *Acc. Chem. Res.* **2014**, *47*, 1097−1105.
(13) Liang, M.; Fan, K.; Pan, Y.; Jiang, H.; Wang, F.; Yang, D.; Lu, D.; Feng, J.; Zhao, J.; Yang, L.; Yan, X. *Anal. Chem.* **2013**, *85*, 308−312.
(14) Zhuang, J.; Fan, K.; Gao, L.; Lu, D.; Feng, J.; Yang, D.; Gu, N.; Zhang, Y.; Liang, M.; Yan, X. *Mol. Pharmaceutics* **2012**, *9*, 1983−1989.
(15) Fan, K.; Wang, H.; Xi, J.; Liu, Q.; Meng, X.; Duan, D.; Gao, L.; Yan, X. *Chem. Commun.* **2017**, *53*, 424−427.
(16) Song, Y.; Qu, K.; Zhao, C.; Ren, J.; Qu, X. *Adv. Mater.* **2010**, *22*, 2206−2210.
(17) Xue, T.; Peng, B.; Xue, M.; Zhong, X.; Chiu, C.-Y.; Yang, S.; Qu, Y.; Ruan, L.; Jiang, S.; Dubin, S.; Kaner, R. B.; Zink, J. I.; Meyerhoff, M. E.; Duan, X.; Huang, Y. *Nat. Commun.* **2014**, *5*, 3200.
(18) Vernekar, A. A.; Sinha, D.; Srivastava, S.; Paramasivam, P. U.; D'Silva, P.; Mugesh, G. *Nat. Commun.* **2014**, *5*, 5301.
(19) Wu, G.-W.; He, S.-B.; Peng, H.-P.; Deng, H.-H.; Liu, A.-L.; Lin, X.-H.; Xia, X.-H.; Chen, W. *Anal. Chem.* **2014**, *86*, 10955−10960.
(20) Zhao, Y.; Huang, Y.; Zhu, H.; Zhu, Q.; Xia, Y. *J. Am. Chem. Soc.* **2016**, *138*, 16645−16654.
(21) He, W.; Liu, Y.; Yuan, J.; Yin, J.-J.; Wu, X.; Hu, X.; Zhang, K.; Liu, J.; Chen, C.; Ji, Y.; Guo, Y. *Biomaterials* **2011**, *32*, 1139−1147.
(22) Xia, X.; Zhang, J.; Lu, N.; Kim, M. J.; Ghale, K.; Xu, Y.; McKenzie, E.; Liu, J.; Ye, H. *ACS Nano* **2015**, *9*, 9994−10004.
(23) Wang, C.-I.; Chen, W.-T.; Chang, H.-T. *Anal. Chem.* **2012**, *84*, 9706−9712.
(24) Duan, D.; Fan, K.; Zhang, D.; Tan, S.; Liang, M.; Liu, Y.; Zhang, J.; Zhang, P.; Liu, W.; Qiu, X.; Kobinger, G. P.; Gao, G. F.; Yan, X. *Biosens. Bioelectron.* **2015**, *74*, 134−141.
(25) Wei, H.; Wang, E. *Anal. Chem.* **2008**, *80*, 2250−2254.
(26) Cheng, H. J.; Lin, S. C.; Muhammad, F.; Lin, Y. W.; Wei, H. *ACS Sens.* **2016**, *1*, 1336−1343.
(27) Cheng, H. J.; Zhang, L.; He, J.; Guo, W. J.; Zhou, Z. Y.; Zhang, X. J.; Nie, S. M.; Wei, H. *Anal. Chem.* **2016**, *88*, 5489−5497.
(28) Hu, Y.; Cheng, H.; Zhao, X.; Wu, J.; Muhammad, F.; Lin, S.; He, J.; Zhou, L.; Zhang, C.; Deng, Y.; Wang, P.; Zhou, Z.; Nie, S.; Wei, H. *ACS Nano* **2017**, *11*, 5558−5566.
(29) Wang, X. Y.; Cao, W.; Qin, L.; Lin, T. S.; Chen, W.; Lin, S. C.; Yao, J.; Zhao, X. Z.; Zhou, M.; Hang, C.; Wei, H. *Theranostics* **2017**, *7*, 2277−2286.
(30) Wang, X. Y.; Hu, Y. H.; Wei, H. *Inorg. Chem. Front.* **2016**, *3*, 41−60.
(31) Wang, Y.; Zhao, M.; Ping, J.; Chen, B.; Cao, X.; Huang, Y.; Tan, C.; Ma, Q.; Wu, S.; Yu, Y.; Lu, Q.; Chen, J.; Zhao, W.; Ying, Y.; Zhang, H. *Adv. Mater.* **2016**, *28*, 4149−4155.
(32) Zhao, M.; Wang, Y.; Ma, Q.; Huang, Y.; Zhang, X.; Ping, J.; Zhang, Z.; Lu, Q.; Yu, Y.; Xu, H.; Zhao, Y.; Zhang, H. *Adv. Mater.* **2015**, *27*, 7372−7378.
(33) He, L. C.; Liu, Y.; Liu, J. Z.; Xiong, Y. S.; Zheng, J. Z.; Liu, Y. L.; Tang, Z. Y. *Angew. Chem., Int. Ed.* **2013**, *52*, 3741−3745.
(34) Zhao, S.; Wang, Y.; Dong, J.; He, C.-T.; Yin, H.; An, P.; Zhao, K.; Zhang, X.; Gao, C.; Zhang, L.; Lv, J.; Wang, J.; Zhang, J.; Khattak, A. M.; Khan, N. A.; Wei, Z.; Zhang, J.; Liu, S.; Zhao, H.; Tang, Z. *Nat. Energy* **2016**, *1*, 16184.
(35) Makiura, R.; Motoyama, S.; Umemura, Y.; Yamanaka, H.; Sakata, O.; Kitagawa, H. *Nat. Mater.* **2010**, *9*, 565−571.
(36) Ai, L.; Li, L.; Zhang, C.; Fu, J.; Jiang, J. *Chem. - Eur. J.* **2013**, *19*, 15105−15108.
(37) Li, B.; Chen, D.; Wang, J.; Yan, Z.; Jiang, L.; Duan, D.; He, J.; Luo, Z.; Zhang, J.; Yuan, F. *Sci. Rep.* **2015**, *4*, 6759.
(38) Wang, Y.; Zhu, Y.; Binyam, A.; Liu, M.; Wu, Y.; Li, F. *Biosens. Bioelectron.* **2016**, *86*, 432−438.
(39) Feng, D.; Gu, Z.-Y.; Li, J.-R.; Jiang, H.-L.; Wei, Z.; Zhou, H.-C. *Angew. Chem., Int. Ed.* **2012**, *51*, 10307−10310.
(40) Whitelock, J. M.; Iozzo, R. V. *Chem. Rev.* **2005**, *105*, 2745−2764.
(41) Guo, C.; Wang, B.; Wang, L.; Xu, B. *Chem. Commun.* **2012**, *48*, 12222−12224.
(42) Guo, C. L.; Fan, X.; Qiu, H.; Xiao, W. Y.; Wang, L. C.; Xu, B. Q. *Phys. Chem. Chem. Phys.* **2015**, *17*, 13301−13306.
(43) Qi, H.; Zhang, L.; Yang, L.; Yu, P.; Mao, L. *Anal. Chem.* **2013**, *85*, 3439−3445.
(44) Ding, Y.; Shi, L.; Wei, H. *Chem. Sci.* **2015**, *6*, 6361−6366.
(45) Hu, Y.; Guo, W.; Ding, Y.; Cheng, H.; Wei, H. *Biosens. Bioelectron.* **2016**, *86*, 858−863.
(46) Wright, A. T.; Zhong, Z. L.; Anslyn, E. V. *Angew. Chem., Int. Ed.* **2005**, *44*, 5679−5682.
(47) Hoffman, M. P.; Engbring, J. A.; Nielsen, P. K.; Vargas, J.; Steinberg, Z.; Karmand, A. J.; Nomizu, M.; Yamada, Y.; Kleinman, H. K. *J. Biol. Chem.* **2001**, *276*, 22077−22085.
(48) Weitz, J. I. *N. Engl. J. Med.* **1997**, *337*, 688−698.
(49) Hirsh, J.; Raschke, R. *Chest* **2004**, *126*, 188S−203S.
(50) Estes, J. W. *Ann. N. Y. Acad. Sci.* **1971**, *179*, 187−204.
(51) Frydman, A. *Pathophysiol. Haemostasis Thromb.* **1996**, *26*, 24−38.
(52) Deswart, C. A. M.; Nijmeyer, B.; Roelofs, J. M. M.; Sixma, J. J. *Blood* **1982**, *60*, 1251−1258.

DOI: 10.1021/acs.analchem.7b02895
Anal. Chem. 2017, 89, 11552−11559